Journal of Organometallic Chemistry 745-746 (2013) 470–478

Contents lists available at ScienceDirect

Journal of Organometallic Chemistry

journal homepage: www.elsevier.com/locate/jorganchem

A new zwitterionic, water soluble, Re(I) complex: Synthesis, spectroscopic and computational characterization

Héctor H. Martinez Saavedra [a], Carlos A. Franca [b], Gabriela Petroselli [c], Rosa Erra-Balsells [c], Gustavo T. Ruiz [a], Ezequiel Wolcan [a,*]

[a] Instituto de Investigaciones Fisicoquímicas Teóricas y Aplicadas (INIFTA, UNLP, CCT La Plata-CONICET), Diag. 113 y 64, B1906ZAA La Plata, Argentina
[b] CEQUINOR (UNLP, CCT La Plata-CONICET), 47 y 115, C. C. 962, 1900 La Plata, Argentina
[c] CIHIDECAR-CONICET, Departamento de Química Orgánica, Facultad de Ciencias Exactas y Naturales, Universidad de Buenos Aires, Pabellón II, 3er P., Ciudad Universitaria, 1428 Buenos Aires, Argentina

ARTICLE INFO

Article history:
Received 31 July 2013
Received in revised form
20 August 2013
Accepted 21 August 2013

Keywords:
Re(I) complex
Zwitterionic
MLLCT
TD-DFT
Acid–base equilibriums

ABSTRACT

A new water soluble Re(I) complex with a zwitterionic structure, $Bu_4N[(bpy)Re(CO)_3(dcbpy)]$ (where Bu = butyl; bpy = 4,4′-bipyridine; dcbpy = 2,2′-bipyridine-5,5′-dicarboxylate), was successfully synthesized and characterized by elemental analysis, ^1H NMR, FTIR and ESI. Protonation studies in aqueous solutions of the Re(I) complex showed three acid–base equilibriums with $pK_{a1} = 5.0$, $pK_{a2} = 3.0$ and $pK_{a3} = 2.0$. pK_{a1} was assigned to the protonation equilibrium at bpy while pK_{a2} and pK_{a3} could be ascribed to protonation/deprotonation of the two carboxylates groups in the dcbpy ligand. With the aid of TD-DFT calculations the nature of the electronic transitions responsible for the pH-dependent UV–vis spectroscopy of the Re(I) complex was identified. At pH = 7 the lower energy band of the complex has $MLLCT_{Re(CO)3\rightarrow dcbpy}$ character while at pH < 2 it switches to $MLLCT_{Re(CO)3\rightarrow bpy}$. This change in the nature of the lower energy band is responsible for the overall spectral changes in the 350–500 nm range after protonation of the Re(I) complex.

1. Introduction

Luminescent transition metal complexes have been utilized as photosensitizers in areas such us solar energy conversion, electron transfer studies, chemiluminescent and electroluminescent systems, binding dynamics of heterogeneous media and probes of macromolecular structure [1]. In this regard, the spectroscopy, photochemistry and photophysics of Re(I) carbonyl–diimine complexes *fac*-ReX(CO)$_3$(α-diimine) continue to attract much research interest ever since their intriguing excited state properties were first recognized in the mid-1970s [2].

Depending on the nature of the axial X ligand *fac*-ReX(CO)$_3$(α-diimine) complexes are often strong luminophores, either in fluid solutions or in low-temperature glasses. The accessible excited states, Re(I) to α-diimine metal-to-ligand charge transfer (MLCT), metal-ligand-to-ligand charge transfer (MLLCT), ligand-to-ligand charge transfer (LLCT), and/or intra ligand (IL) excited states, are generally involved with the observed luminescence of these complexes at room temperature. A rational design in the synthesis of the α-diimine ligands was used to tune the photophysical and photochemical properties of the metal complexes in order to obtain photosensitizers that might be utilized in broad research areas such as electron transfer studies [3], solar energy conversion [4–6] and catalysis [7]. Possible applications as luminescent sensors [8–10], molecular materials for non-linear optics [11,12] or optical switching [13] have also emerged. In particular, luminescent transition metal complexes of Re(I) and Ru(II) with polypyridyl ligands have been recognized as good candidates for the development of pH sensing devices [14–16]. As these complexes show exceptionally rich excited-state behavior and redox chemistry as well as thermal and photochemical stability [17,18], they have also been used as biological labeling reagents and non-covalent probes for biomolecules and ions [19–21]. Moreover, there are potential biochemical and technical applications based on the formation of adducts between transition metal complexes of Re(I), and biological macromolecules such as DNA [22,23].

One of the major disadvantages of *fac*-ReX(CO)$_3$(α-diimine) complexes when applied to biological media is connected to their usually very low solubility in water at physiological pH. In fact, there are a very limited number of water soluble *fac*-ReX(CO)$_3$(α-

* Corresponding author.
E-mail address: ewolcan@inifta.unlp.edu.ar (E. Wolcan).

0022-328X/$ – see front matter © 2013 Elsevier B.V. All rights reserved.
http://dx.doi.org/10.1016/j.jorganchem.2013.08.038

diimine) complexes [14,16,24–29] compared to the huge number of Re(I) carbonyl–diimine complexes reported to be soluble exclusively in organic solvents. In previous work, we have characterized a water soluble Re(I) tricarbonyl complex including a biological relevant ligand like pterin in its structure [29]. In this paper, we present the synthesis of a new water soluble Re(I) tricarbonyl complex coordinating the ligand 2,2′-bipyridine-5,5′-dicarboxylate (dcbpy). The Re(I) complex, namely $Bu_4N[(bpy)Re(CO)_3(dcbpy)]$ (where bpy = 4,4′-bipyridine) was characterized by ^1H NMR, FTIR, ESI and elemental analysis. It has a zwitterionic structure where the two negative charges of the carboxylate groups are balanced by the positive charges of the Re(I) center and that of a tetrabutyl ammonium cation. To complete the Re(I) complex characterization, protonation studies were performed in its aqueous solutions by following the behavior of UV–vis absorption spectra upon pH change, within the 1–7 pH range. With the aid of chemometric methods, three pK_a values could be obtained from the protonation studies that were assigned to the protonation of bpy ligand ($pKa_1 = 5.0$) and to the acid–base equilibrium of the two carboxylate groups ($pKa_2 = 3.0$ and $pKa_3 = 2.0$). TD-DFT calculations helped to identify the nature of the electronic transitions in the UV–vis spectroscopy of the Re(I) complex aqueous solutions. At neutral pH the lower energy band of the complex has $MLLCT_{Re(CO)3\rightarrow dcbpy}$ character while at pH = 1 it switches to $MLLCT_{Re(CO)3\rightarrow bpy}$. This change in the nature of the lower energy band is responsible for the overall spectral changes in the 350–500 nm range after protonation of the Re(I) complex.

2. Materials and methods

HPLC grade methanol, ethanol, ethyl ether, iso-octane and acetonitrile (J. T. Baker, USA), were used without further purification. 2,2′-bipyridine-5,5′-dicarboxylic acid (H_2dcbpy), 4,4′-bipyridine (bpy), NaH_2PO_4, Na_2HPO_4, tetrabutyl ammonium hydroxide (Bu_4NOH) methanolic solution (1 M) and $ClRe(CO)_5$ were purchased from Sigma–Aldrich Chemical Co., USA at the highest purity available and were used as received. Water of very low conductivity (Milli Q grade) was used. UV–vis spectra were recorded on a Shimadzu UV-1800 spectrophotometer. pH measurements were performed with an ADWA model AD8000 pH meter using an A1131B glass electrode (pH range: 0–13). FTIR spectra were recorded on a Nicolet 8700 Thermo Scientific. ^1H NMR spectra of the Re(I) complex solutions were recorded at 300 K with a Bruker AM-500 spectrometer operating at 500 MHz. [D6]DMSO was used as a solvent and the chemical shifts were referenced relative to the $(CH_3)_2SO$ in [D6]DMSO ($\delta = 2.54$ ppm). Typically, solutions were introduced into a 5 mm diameter tube.

2.1. Synthesis

The chemical structures of the materials used in this work and the synthetic routes are depicted in Scheme 1. The Re(I) dcbpy coordinated complex was prepared by a modification of procedures reported for the synthesis of similar Re complexes [14,25,28,30]. A 100 ml round-bottomed flask was loaded with 150 mg (6.1×10^{-4} mol) of H_2dcbpy, 85 ml of methanol and 1.35 ml (1.35×10^{-3} mol) of a Bu_4NOH methanolic solution (1 M). In this way, H_2dcbpy, which is nearly insoluble in most organic solvents [28], was easily dissolved in methanol by formation of its tetrabutyl ammonium salt, $(Bu_4N)_2$dcbpy. The resulting colorless solution was heated at around 70 °C. Then, 221 mg (6.1×10^{-4} mol) of $ClRe(CO)_5$ were slowly added to the vigorously stirred hot methanolic solution. The initially colorless liquid turned to red during the 9 h that the reaction mixture was refluxed under a blanket of N_2. The solution was then cooled to room temperature, and evaporated to a ~2 ml orange oil. This orange oil was then dissolved in acetonitrile (220 ml) along with 164.5 mg (6.1×10^{-4} mol) of $AgCF_3SO_3$. The mixture was refluxed at 70 °C in the darkness under a blanket of N_2 during 4 h. After evaporation of the reaction mixture to dryness, the resulting brown-dark solid mass was suspended in 60 ml of methanol, and a dark-brown precipitate, containing AgCl, was filtered-off and washed several times with methanol. The resulting red 100 ml methanolic solution was then loaded with 952 mg (6.1×10^{-3} mol) of bpy. The resulting mixture was then refluxed overnight in the darkness at 70 °C under a blanket of N_2. After evaporation of the solution to dryness, the orange-yellow solid mass was washed with ethyl ether repeatedly to eliminate the excess of the bpy ligand. The resulting solid was re-dissolved in a minimum volume of dichloromethane, and the complex was precipitated by the slow addition of cold iso-octane. The re-

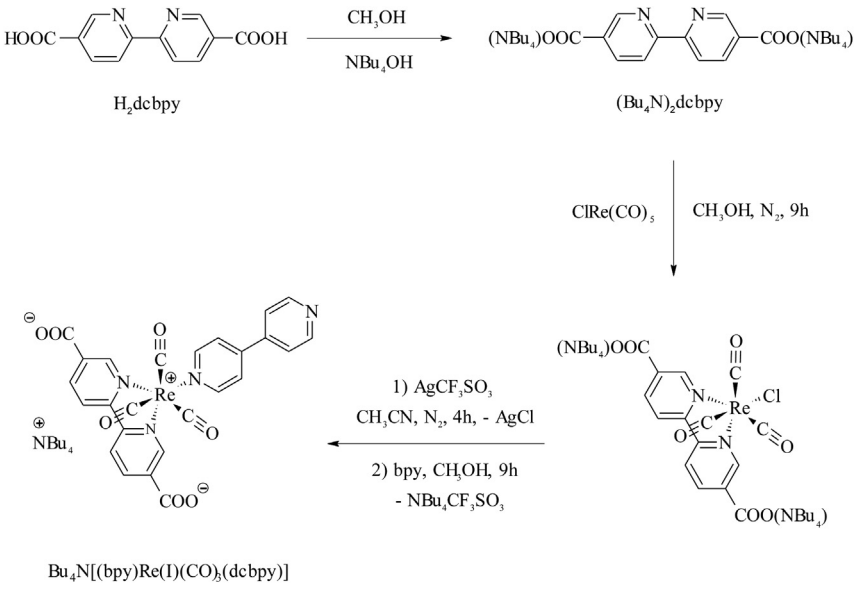

Scheme 1. Synthetic route for $Bu_4N[(bpy)Re(CO)_3(dcbpy)]$.

crystallization procedure was repeated until a constant value was obtained for the molar absorption coefficient. The obtained orange solid was dried under vacuum. Yield, 500 mg (60%). Anal. Calcd. for $Bu_4N[(bpy)Re(CO)_3(dcbpy)].4H_2O$·(Molecular Formula $C_{41}H_{58}N_5O_{11}Re$): C, 50.09; H, 5.95; N, 7.12. Found: C, 50.5 ± 0.3; H, 6.0 ± 0.2; N, 6.9 ± 0.3. IR (KBr, cm^{-1}): 1344 (m), 1624 (m), 1890 (s), 1915 (s), 2019 (s), 2963 (m), 3415 (m, broad). ^1H NMR (500 mHz, [D6]DMSO): δ = 9.32–9.28 (m), δ = 8.74 (d, J = 6 Hz, 2H, H_δ bpy), δ = 8.63 (m), δ = 8.49 (m), 7.85 ppm (d, J = 6 Hz, 2H, H_γ bpy), 3.13 (t, J = 7.5 Hz, 8H, N-($\underline{CH_2}$–CH_2–CH_2–CH_3)$_4$), 1.54 (m, 8H, N–(CH_2–$\underline{CH_2}$–CH_2–CH_3)$_4$), 1.27 (m, 8H, N–(CH_2–CH_2–$\underline{CH_2}$–CH_3)$_4$) and 0.88 (t, J = 7.2 Hz, 12H, N–(CH_2–CH_2–CH_2–$\underline{CH_3}$)$_4$).

2.2. ESI–MS analysis

ESI–MS analyses were performed in positive ion mode using mass spectrometer BRUKER MICROTOF-Q II equipped with CID. The capillary temperature was 180 °C. Stock solutions of the complex were prepared in methanol at a concentration 10^{-4} M. Diluted solutions were prepared from the stock solutions. High flow electrospray with an assistance of corona discharge taking place at the tip of the electrospray capillary was used to avoid decomposition (interchange of ligands and solvent) of the Re(I) complex and to induce ionization of neutral analytes [31–33]. The source voltage applied was 8 kV, the source current 15 μA, the sheath gas flow rate was 30 (a.u.) and the capillary temperature was 150 °C. Ion optics parameters: multipole 00 offset: −3.3 V, lens 0: −6.2 V, multipole 0 offset: ±6.3 V, lens 1: −9.2 V, gate lens: −91.9 (V), multipole 1 offset: −6.6 (V) and multipole RF amplitude: 602.3 (Vp-p). A syringe pump (Agilent, USA) with 2.3 mm in diameter was used to introduce the sample at a flow rate of 10 μl/min and methanol. Each experiment was repeated at least three times in order to ensure reproducibility. Spectra were obtained and analyzed with the program Thermo XcaliburQual Browser.

2.3. Protonation studies and spectroscopic analysis

pK_a values were determined by spectrophotometric pH titrations using NaH_2PO_4/Na_2HPO_4 (each 0.1 M) buffer. In each experiment, 50 ml of solution containing the Re(I) complex ([Re] = 3×10^{-5} M), initially at pH = 6.7, were turned to pH = 7 by addition of 3M NaOH. After that, the pH was gradually lowered to pH = 1 by addition of 50 or 100 μl aliquots of 3 M $HClO_4$, and then the absorption spectrum of each solution was recorded. The procedure was repeated reversing the pH from 1 to 7 by adding 50–100 μL aliquots of 3 M NaOH. When it was necessary, the absorbances were corrected by the appropriate dilution factors. We used chemometric-techniques [34] in order to retrieve, from the absorbance matrix, the concentration profiles and the spectra of each contributing species [35,36]. These methods can be applied to bilinear spectroscopic data from a chemical reaction to provide information about composition changes in an evolving system. In the present work we used the alternating least-squares (ALS) algorithm to simultaneously estimate concentration and spectral profiles [37]. ALS extracts useful information from the experimental data matrix $\boldsymbol{A}(i \times j)$ by the iterative application of the following matrix product: $\boldsymbol{A} = \boldsymbol{C}\boldsymbol{S}^T + \boldsymbol{E}$ where $\boldsymbol{C}(i \times n)$ is the matrix of the concentrations profiles; $\boldsymbol{S}^T(n \times j)$ is that containing the spectral profiles, and $\boldsymbol{E}(i \times j)$ represents the error matrix. The indexes i, n and j denote the sampling pHs, absorbing species and recorded wavelengths, respectively. Resolving matrix $\boldsymbol{A}$ may be a rather difficult task [38] since on the one hand, n is usually unknown [39] and on the other hand, curve resolution methods cannot deliver a single solution because of rotational and scale ambiguities [40]. We applied Factor Analysis and Singular Value Decomposition to the experimental matrix for the estimation of n. In order to reduce rotational ambiguities we used some chemically relevant constraints [41] such as non-negativity, closure, selectivity and unimodality.

2.4. Computational details

The electronic structure of Re(I) tricarbonyl complexes were determined using tools of DFT [42–44] as implemented in Gaussian 09 package [45], using the three-parameter hybrid functional developed by Becke [46] in conjunction with the LYP [47] exchange potential (B3LYP) with the LanL2DZ basis set which uses Dunning D95V basis set on C, N, O, H [48] and Los Alamos ECP plus DZ on Re [49–51]. Vibrational frequencies were computed at the same level of theory to confirm that these structures were minima on the energy surfaces. The vertical transition energies were calculated at the optimized ground-state geometry using TD-DFT [52–54] at the same level of theory for the four protonation states of the Re(I) complex (see below). Both optimized geometries and UV–vis calculations were carried out including solvent effects (water) through the Polarizable Continuum Model [55–57] as implemented in the Gaussian 09 package to produce a number of 80 singlet-to-singlet transitions.

3. Results and discussion

3.1. Spectroscopic characterization

The Re complex was obtained in good yield and it was characterized by elemental analysis, FTIR, ^1H NMR, and electrospray ionization mass spectrometry spectra. The substance IR absorption spectrum is consistent with both the facial configuration of the carbonyl ligands and with its C_s symmetry, as revealed by the presence of the two intense absorptions bands which are observed in the 2050–1880 cm^{-1} region. According to previous reports on similar compounds, the sharp band at higher frequency (about 2019 cm^{-1}) is attributed to the 1A′ mode (totally symmetric in-phase stretching of the three CO ligands), whereas the remaining two bands at intermediate and lower frequencies (1915 and 1890 cm^{-1}), are assigned to the 2A′ (totally symmetric out-of-phase stretching) and A″ modes (asymmetric stretching of the equatorial CO ligands) [15,29,58]. The presence of Bu_4N^+ in the structure of the complex is witnessed by the frequencies at 1344 and 2963 cm^{-1} which correspond to C–H of CH_3 stretching vibration and by the one at 1624 cm^{-1} which is indicative of the bending stretching of the quaternary ammonium group [59]. The broad feature at 3415 cm^{-1} is indicative of –OH stretching due to the presence of crystallization water molecules.

^1H NMR spectra shows, among others, the two typical doublet signals from bpy at δ 8.74 and 7.85 ppm that according to the literature [60] can be assigned to H_δ and H_γ, respectively. ^1H NMR signals corresponding to the 6H of the dcbpy ring and to the 4H (H_α and H_β) of the bpy ring appeared as very broad and badly resolved in the δ = 8.43–9.40 ppm range and could not unequivocally be assigned to the Re(I) complex structure. Signals of Bu_4N^+ ligand were detected at δ = 3.13, 1.54 and 1.27 ppm, methylene moiety each, and δ = 0.88 ppm corresponding to the methyl group. Surface integration ratio between H_δ:H_γ:N–$(CH_2)_4$– signals was 1:1:4.

Fig. S1 shows positive ion ESI mass spectra of $Bu_4N[(bpy)Re(CO)_3(dcbpy)]$, (M), in methanol. The intact molecular ion of the complex, M was detected as protonated [M + H^+] and sodiated form [M + Na^+] at m/z = 912.33 and m/z = 934.31, respectively. Additionally, the Re complex with one additional Bu_4N^+, as [M + Bu_4N^+] was observed at m/z = 1153.61. Furthermore, signals observed at m/z = 693.03 and m/z = 715.01 correspond to [M −

$Bu_4N^+ + Na^+$] and [M − $Bu_4N^+ + 2Na^+$], respectively. MS–MS spectra were recorded. Most intense signal produced by fragmentation of $m/z = 934.31$ was observed at $m/z = 796.25$ (Spectrum not shown).

Moreover, ESI mass spectra were recorded after the addition of Bu_4NPF_6 to the methanolic solution of the rhenium complex. In this experiments the signals detected with higher intensity were $m/z = 1153.61$, $m/z = 968.88$ (cluster of four Bu_4N^+) and $m/z = 934.31$.

The most intense signal was observed at $m/z = 1153.61$ and correspond to a chemical formula of $C_{57}H_{86}O_7N_6Re$. As mentioned before this signal corresponds to the Re complex with one additional Bu_4N^+ moiety. Elemental analysis and ^1H NMR spectra showed that the complex has, in its structure, only one Bu_4N^+ unit. The species detected by ESI–MS at $m/z = 1153.61$ could be formed in the solution due to an exchange of the Bu_4N^+ cation between two molecules of the complex before the ionization took place, as shown in the following reaction scheme:

$$2\ Bu_4N[(bpy)Re(CO)_3(dcbpy)] \rightarrow (Bu_4N)_2[(bpy)Re(CO)_3(dcbpy)]^+ + [(bpy)Re(CO)_3(dcbpy)]^-$$

3.2. UV–vis spectroscopy

The absorption spectrum of $Bu_4N[(bpy)Re(CO)_3(dcbpy)]$ in neutral solutions, i.e. at pH = 7, consists of four strong absorption bands ($\varepsilon \sim 2 \times 10^4\ M^{-1}\ cm^{-1}$) centered at $\lambda_{max} = 251$, 290, 316 and 332 nm and a weaker band of medium intensity ($\varepsilon \sim 3 \times 10^3\ M^{-1}\ cm^{-1}$) that appears as a shoulder centered at ~362 nm. In acidic media (pH = 1) the band at $\lambda_{max} = 290$ nm shifts to 295 nm and experiences an intensity enhancement compared to the neutral solution while the bands at 251, 316 and 332 nm hardly experience any wavelength shift though they suffer an intensity increase. The low energy shoulder, however, shifts to 376 nm at acidic pH. A reversible protonation/deprotonation behavior is found in the UV–vis spectrum of the Re(I) complex as a function of the pH upon addition of $HClO_4$ from pH = 7 to pH = 1. Those spectral changes can be reversed by addition of NaOH from pH = 1 backward to pH = 7.

We measured the UV–vis spectrum of $Bu_4N[(bpy)Re(CO)_3(dcbpy)]$ in NaH_2PO_4/Na_2HPO_4 buffer solutions at room temperature and titrations were carried out by adding aqueous $HClO_4$ to observe spectral changes (see Fig. 1). Fig. 1a shows the spectral changes observed between pH = 7 and pH = 4, in a pH region where the spectral changes were very moderate. However, three isosbestic points at 242, 287 and 314 nm could be identified in that region. The spectral changes observed between pH = 4 and pH = 1 (Fig. 1b) were more noticeable than those between pH = 7 and pH = 4. Between pH = 2.8 and pH = 1, an isosbestic point could be identified at 285 nm, while at the intermediate pHs, i.e. between pH = 3 and pH = 4, no isosbestic points are present. This behavior is indicative of the existence of various protonated/deprotonated species in simultaneous equilibriums. Therefore, we decided to apply chemometric techniques in the analysis of the full matrix of UV–vis spectra of Fig. 1a and b to get an estimation of the p*K*a values for the corresponding acid/base equilibriums. Both Factor Analysis and Singular Value Decomposition were used for the estimation of the number of independent contributions yielding *n* values of 4. Orthogonal projection approach was used to obtain initial guesses of the spectra corresponding to each contributing species [61]. The spectral shapes obtained by using a multivariate curve resolution-alternating least squares (MCR-ALS) method for the four species are shown in Fig. 2. Fig. 2 also shows the distribution functions for the four species over the whole pH range. From this figure, three p*K*a values can be obtained, i.e. 2.0, 3.0 and 5.0. According to literature reports, the pyridinic free nitrogen of coordinated bpy ligand is supposed to be more basic than carboxy substituents in coordinated dcbpy ligand. For instance, the dissociation of carboxylic protons in (2,2′-bpy-4,4′-dicarboxylic acid) Ru(II) complexes was found to occur in two steps with pKa_1 ranging between 2.8 and 3 and pKa_2 in the range 1.5–1.8 [62,63] while for (2,2′-bpy-5,5′-dicarboxylic acid) Ru(II) complexes a single p*K*a ~ 2.8 [62] was identified. On the other hand, the proton dissociation pK_a in heteroleptic Ru(II) complexes coordinating the bpy ligand was reported to be 4.5 [64]. On this basis the three p*K*a values obtained for $Bu_4N[(bpy)Re(CO)_3(dcbpy)]$ can be assigned to the protonation of bpy ligand ($pKa_1 = 5.0$) and to the acid–base equilibrium of the two carboxylate groups ($pKa_2 = 3.0$ and $pKa_3 = 2.0$). The three pK_a values thus obtained for the $Bu_4N[(bpy)$

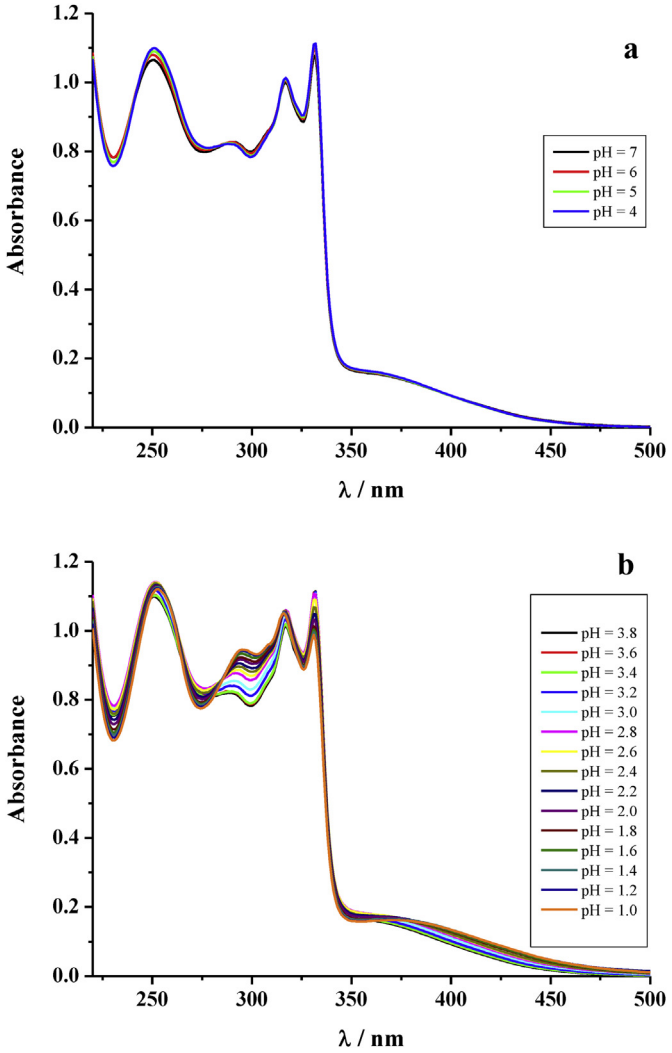

Fig. 1. UV–vis spectral changes experienced by $Bu_4N[(bpy)Re(CO)_3(dcbpy)]$ complex in protonation studies. (a) Spectral changes in the 4–7 pH range. (b) Spectral changes in the 3.8–1 pH range. See text for details.

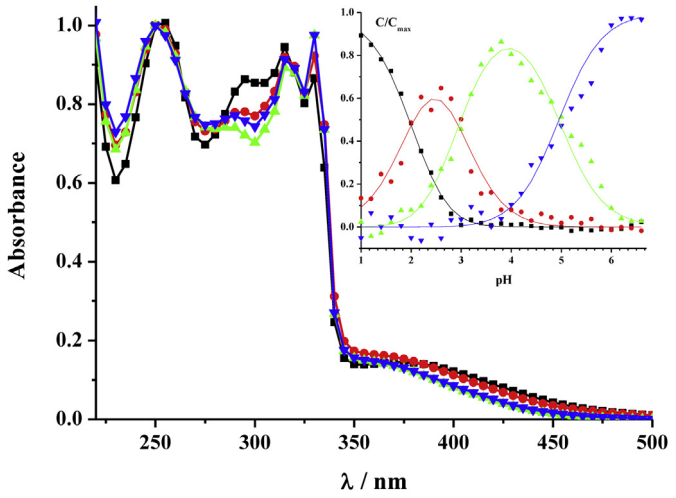

Fig. 2. Spectral shapes and distribution functions obtained from chemometric analysis of Fig. 1a and b for the pH-dependent species of the Re(I) complex: **(ReL)**$^-$ (blue down triangles), **(ReL)H** (green up triangles), **(ReL)H$_2^+$** (red circles) and **(ReL)H$_3^{2+}$** (black squares). See text for details. (For interpretation of the references to colour in this figure legend, the reader is referred to the web version of this article.)

$Re(CO)_3$(dcbpy)] agree well with the pK_a values reported for [(bpy)$Re(CO)_3$(2,2′-bpy-4,4′-dicarboxylic acid)]CF_3SO_3 [25].

3.3. DFT and TD-DFT calculations

Density Functional Theory (DFT) and Time-Dependent Density Functional Theory (TD-DFT) calculations of ground and excited state properties of a series of Re(I) tricarbonyl complexes have been recently employed to interpret the experimental absorption bands arisen from a set of MLCT, LLCT and IL transitions [65–73].

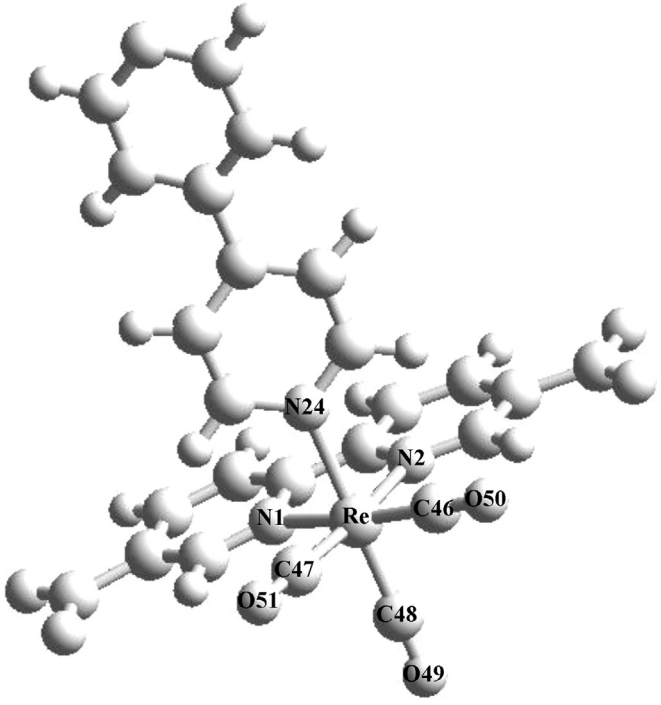

Fig. 3. Molecular plot from DFT calculations of [(bpy)$Re(CO)_3$(dcbpy)]$^-$ showing the labeling of some relevant atoms that appear in Table 1.

3.3.1. Structural characterization

The optimized ground-state geometry is displayed in Fig. 3 for the bare (un-protonated) complex, i.e. [(bpy)$Re(CO)_3$(dcbpy)]$^-$. The Re(I) ion is in a slightly distorted octahedral environment. The bond lengths, as shown in Table 1, are within normal ranges found in related Re(I) complexes [29,60,65,68,70,74]. A planar substituted bipyridine coordinated to the metal defines an equatorial plane acting as a bidentate ligand [d(Re-N) = 2.176 Å, d(Re-N) = 2.178 Å, ∠(N-Re-N) = 75.7°]. Two CO groups lie at *cis*-positions nearly onto this plane [Re-C distances of 1.926 and 1.925 Å]. The octahedron apical positions are occupied by a third CO group [d(Re-C) = 1.924 Å] and a bpy molecule [d(Re-N) = 2.228 Å]. The bond lengths of Re-N are always longer than the bond lengths of Re-C, being the Re-N(bpy) bond length the longest. Re-(CO) bonds are nearly perpendicular to each other [OC-Re-CO angles in the 89.1–90.4° range]. The optimized ground-state geometry for the fully protonated complex, i.e. [(Hbpy)$Re(CO)_3(H_2$dcbpy)]$^{2+}$ (not shown), is similar to that of [(bpy)$Re(CO)_3$(dcbpy)]$^-$, only a very small increase in Re-N and Re-C bond lengths is observed after protonation (Table 1). In the fully protonated complex, an increase in the Re-N(dcbpy) distances (relative to the un-protonated complex) is accompanied by a decrease in Re(I)-dcbpy angle while the lengthening of the Re-N24 distance always leads to an increase in the (N1-Re-N24) and (N2-Re-N24) angles.

3.3.2. IR and UV–vis spectroscopy

The optimized ground-state geometry of [(bpy)$Re(CO)_3$(dcbpy)]$^-$ was used to calculate the normal mode frequencies which were compared to the experimental IR frequencies observed for Bu_4N[(bpy)$Re(CO)_3$(dcbpy)] in the CO stretching region. Calculated IR frequencies are in good agreement with the experimental values. For instance, the calculated IR frequency for the 1A′ mode, 1977.3 cm^{-1}, compares with the experimental one, 2019 cm^{-1}, with a shift of $\Delta = (\upsilon_{exp} - \upsilon_{calc}) = 41.7$ cm^{-1}. For the 2A′ and A″ modes, the predicted values are 1889.6 cm^{-1} and 1883 cm^{-1}, respectively, which can be compared to the experimental IR frequencies, 1915 cm^{-1} ($\Delta = 25.4$ cm^{-1}) and 1890 cm^{-1} ($\Delta = 7$ cm^{-1}), respectively.

Theoretical calculations in the literature have shown that the highest occupied molecular orbital (HOMO) in *fac*-ReX$(CO)_3$(α-

Table 1
DFT calculated bond lengths (Å) and angles (°) around the Re ion in [(bpy)$Re(CO)_3$(dcbpy)]$^-$, **(ReL)**$^-$, and [(Hbpy)$Re(CO)_3(H_2$dcbpy)]$^{2+}$, **(ReL)H$_3^{2+}$**.

	(ReL)$^-$	(ReL)H_3^{2+}
Bond lengths (Å)		
Re-N1	2.176	2.182
Re-N2	2.178	2.184
Re-N24	2.228	2.231
Re-C46	1.926	1.926
Re-C47	1.925	1.927
Re-C48	1.924	1.929
Bond angles (°)		
N1-Re-N2	75.7	75.4
N1-Re-N24	84.6	85.1
N1-Re-C46	172.6	172.9
N1-Re-C47	97.6	97.9
N1-Re-C48	92.6	92.5
N2-Re-N24	84.9	85.5
N2-Re-C46	97.5	97.9
N2-Re-C47	172.9	173.1
N2-Re-C48	92.2	92.1
C46-Re-N24	92.1	92.1
C46-Re-C47	89.1	88.6
C46-Re-C48	90.4	90.1
C47-Re-N24	92.2	92.1
C47-Re-C48	90.3	90
C48-Re-N24	176.4	177

diimine) complexes corresponds to an orbital mainly localized in the Re center with some delocalization over X ligands. This delocalization also accounts for the mixing of IL and MLCT states. On the other hand, the lowest unoccupied molecular orbital (LUMO) is localized exclusively on the α-diimine ligand [58]. The calculated TD-DFT results are summarized and compared with experimental data in Table 2 for the four protonated species of the Re(I) complex: $[(bpy)Re(CO)_3(dcbpy)]^-$, **(ReL)**$^-$; $[(Hbpy)Re(CO)_3(dcbpy)]$, **(ReL)H**; $[(Hbpy)Re(CO)_3(Hdcbpy)]^+$, **(ReL)H$_2^+$** and $[(Hbpy)Re(CO)_3(H_2dcbpy)]^{2+}$, **(ReL)H$_3^{2+}$**. It is observed that the main spectral features (the four intense UV absorptions and the less intense UV–vis shoulder) for **(ReL)**$^-$, **(ReL)H**, **(ReL)H$_2^+$** and **(ReL)H$_3^{2+}$** are predicted to a great accuracy, both in position and relative intensities, by TD-DFT calculations. Hereafter we compare TD-DFT results for **(ReL)**$^-$ and **(ReL)H$_3^{2+}$**, since the intermediate protonated species, i.e. **(ReL)H** and **(ReL)H$_2^+$**, show similar behavior.

For **(ReL)**$^-$ the main HOMOs involved in the most intense electronic transitions are H-12 (a π orbital delocalized between the Re(I) and the bpy ligand), H-10 (a molecular orbital of the exterior ring of bpy molecule), H-9 (a π orbital delocalized on the dcbpy ligand), H-8 (a σ orbital delocalized in the equatorial plane of the Re(I) bonds) and H-6 and H-7 (π orbitals of Re-C bonds). On the other hand, the main LUMOs of **(ReL)**$^-$ are L and L+2 (π* orbitals of the dcbpy ligand), L+1 (π* orbital of the bpy ligand) and L+4 (π* orbital of the three CO). TD-DFT predicts that the lower energy band of **(ReL)**$^-$, at around 360 nm and predicted at 371 nm, is MLCT in nature with most of the electron density transferred from the Re-C bonds to the dcbpy part of the molecule (See Fig. 4). Since H-6 and H-7 consist mainly of π orbitals of Re-C bonds, this lower energy is not a pure MLCT transition and should be viewed better as a $MLLCT_{Re(CO)3\rightarrow dcbpy}$ transition (i.e. a delocalized $Re(CO)_3$ → dcbpy CT transition). The higher energy band of **(ReL)**$^-$, observed at 252 nm and predicted to be at 255 nm, consists mainly of intra ligand electronic transitions of bpy with some contributions of the Re(I) center. The band at 293 nm (predicted at 290) is a $MLLCT_{Re(CO)3\rightarrow dcbpy}$. The band at 317 is predicted as two bands at around 314 nm being both a sum of intra ligand transitions of dcbpy and bpy. The band at 332 nm, predicted at 327 nm, is mainly a $MLLCT_{Re(CO)3\rightarrow bpy}$.

For the fully protonated species, **(ReL)H$_3^{2+}$**, the relevant HOMOs involved in the most intense electronic transitions are H and H-1 (π orbitals delocalized between the Re-C bonds), H-2 (a σ orbital delocalized between Re-C and Re-N(dcbpy) bonds), H-3 and H-6 (π orbitals delocalized on the dcbpy ligand), and H-7 and H-8 (π orbitals delocalized on the bpy ligand). On the other hand, the main LUMOs of **(ReL)H$_3^{2+}$** are L, L+2 and L+3 (π* orbitals delocalized on

Table 2
Comparison of experimental absorption data with TD-DFT calculations for $(ReL)^-$, $(ReL)H$, $(ReL)H_2^+$ and $ReLH_3^{2+}$.

Compound	λ_{obs}/nm ($\varepsilon/10^3$ M^{-1} cm^{-1})	λ_{calc}/nm (f_{osc})	Electronic transitions (% coefficients)
$(ReL)^-$	252 (34.5)	255.51 (0.544)	H-12 → L+1 (94%)
		258.53 (0.094)	H-8 → L+4 (36%), H-6 → L+10 (12%), H-13 → L+1 (9%), H-8 → L+3 (4%)
		273.39 (0.056)	H-11 → L+1 (19%), H-4 → L+3 (19%), H-3 → L+3 (13%), H-8 → L+2 (6%)
	293 (27.4)	290.26 (0.063)	H-8 → L+4 (14%), H-7 → L+2 (43%), H-7 → L+6 (19%), H-9 → L (3%)
	317 (33.3)	314.47 (0.155)	H-10 → L+1 (44%), H-9 → L (30%), H-8 → L+1 (18%)
		314.69 (0.245)	H-10 → L+1 (26%), H-9 → L (57%), H-8 → L+1 (7%), H-7 → L+2 (4%)
	332 (35.9)	327.33 (0.160)	H-6 → L+1 (75%), H-7 → L+1 (6%), H-5 → L+1 (5%), H-3 → L+1 (5%)
		337.31 (0.065)	H-6 → L+1 (12%), H-5 → L+1 (26%), H-3 → L+1 (26%), H-2 → L+1 (29%)
	361 (5.2)	370.77 (0.079)	H-6 → L (82%), H-7 → L (9%), H-3 → L (3%), H-2 → L (3%)
(ReL)H	252 (36.6)	243.24 (0.078)	H-15 → L (92%)
		250.61 (0.071)	H-14 → L (72%)
		259.00 (0.202)	H-12 → L (91%)
		264.49 (0.252)	H-11 → L (86%)
		265.31 (0.11)	H-7 → L+5 (14%), H-6 → L+4 (22%), H-6 → L+5 (10%), H-6 → L+8 (13%)
		265.86 (0.057)	H-7 → L+4 (21%), H-8 → L+3 (9%)
	293 (27.1)	288.99 (0.089)	H-10 → L (25%), H-8 → L+6 (10%), H-6 → L+3 (20%), H-6 → L+8 (15%)
	317 (33.8)	314.89 (0.392)	H-9 → L+1 (88%)
	331 (37.0)	365.71 (0.085)	H-7→L+1 (91%)
	361 (5.4)	410.98 (0.152)	H-7 → L (94%)
$(ReL)H_2^+$	252 (38.0)	250.90 (0.087)	H-6 → L+6 (31%), H-6 → L+8 (35%)
		259.22 (0.36)	H-10 → L (58%), H-3 → L+7 (10%)
		259.33 (0.083)	H-9 → L (62%)
		259.59 (0.066)	H-9 → L (15%), H-4 → L+3 (37%)
		263.39 (0.061)	H-5 → L+5 (13%), H-4 → L+4 (10%), H-4 → L+9 (11%), H-3 → L+6 (15%)
		263.65 (0.057)	H-8 → L (75%)
		271.00 (0.052)	H-8 → L (15%), H-6 → L+2 (14%)
	293 (29.5)	301.59 (0.112)	H-5 → L+2 (13%), H-4 → L+2 (47%)
	317 (35.3)	317.28 (0.255)	H-6 → L+1 (36%), H-3 → L+2 (37%), H-1 → L+2 (12%)
		320.12 (0.126)	H-6 → L+1 (15%), H-1 → L+2 (73%)
	332 (36.4)	328.65 (0.098)	H-6 → L+1 (34%), H-3 → L+2 (54%)
	360 (6.0)	389.75 (0.051)	H-5 → L+1 (65%), H-4 → L+1 (30%)
		412.78 (0.199)	H-3 → L (89%)
$(ReL)H_3^{2+}$	253 (37.3)	252.36 (0.07)	H-8 → L+1 (69%)
		254.09 (0.06)	H-3 → L+2 (69%)
		257.41 (0.45)	H-7 → L+1 (73%)
		259.11 (0.11)	H-2 → L+9 (15%), H-1 → L+5 (19%), H → L+9 (18%)
		260.12 (0.06)	H-6 → L+1 (76%)
		263.90 (0.06)	H-2 → L+6 (20%), H-1 → L+6 (12%), H-1 → L+7 (23%)
	295 (31.5)	295.59 (0.26)	H-3 → L (12%), H-1 → L+3 (15%), H → L+3 (41%)
	316 (35.0)	317.33 (0.26)	H-3 → L (36%), H-1 → L+2 (37%)
	331 (32.9)	329.27 (0.10)	H-3 → L (38%), H-1 → L+2 (43%)
	371 (5.4)	388.74 (0.17)	H-1 → L+1 (22%), H → L+1 (75%)
		451.72 (0.06)	H-1 → L (27%), H → L (71%)

the dcbpy ligand), L+1 (a π^* orbital delocalized on the bpy ligand), and L+6 and L+9 (π^* orbitals centered on the three CO). TD-DFT predicts that the lower energy band of **(ReL)H$_3^{2+}$**, at around 371, and predicted at 389 nm, is $MLLCT_{Re(CO)3\rightarrow bpy}$ in nature. This observation contrasts with the prediction for the lower energy band of **(ReL)**$^-$, which is $MLLCT_{Re(CO)3\rightarrow dcbpy}$ in nature (See Figs. 4 and 5). The higher energy band of **(ReL)H$_3^{2+}$**, observed at 253 nm and predicted to be at 257 nm, is nearly a pure intra ligand electronic transition of bpy with a minor contribution from the dcbpy (the contributions of the Re(I) center which were present in the electronic transition at 252 nm in **(ReL)**$^-$ have disappeared here). The bands at 295, 316 and 331 nm, predicted at 295.6, 317 and 329 nm, respectively, are an admixture of $MLLCT_{Re(CO)3\rightarrow dcbpy}$ and intra ligand transitions of dcbpy. From the above analysis it is evident that protonation of **(ReL)**$^-$ to yield **(ReL)H$_3^{2+}$**, moves the $MLLCT_{Re(CO)3\rightarrow bpy}$ transition from 327 nm (predicted for **(ReL)**$^-$) to 389 nm (predicted for **(ReL)H$_3^{2+}$**).

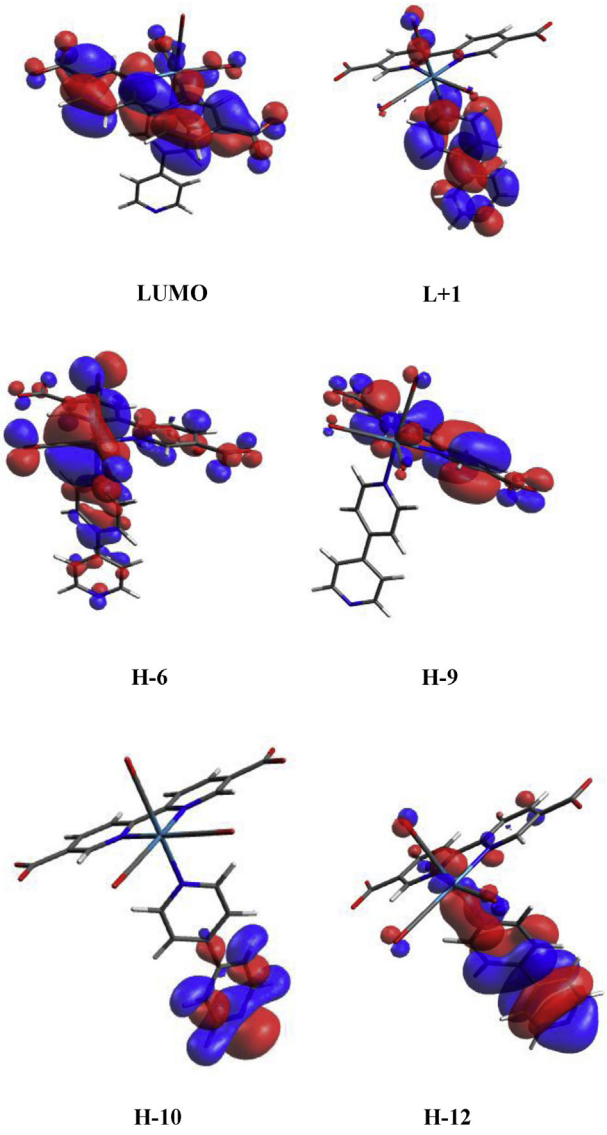

Fig. 4. Molecular orbital diagrams for complex **(ReL)**$^-$. H-6 and LUMO are the major MOs involved in the lower energy transition (λ_{max} = 361 nm), while orbitals L+1, H-9, H-10 and H-12 are the major contributors to the electronic spectrum in the 220–350 nm range.

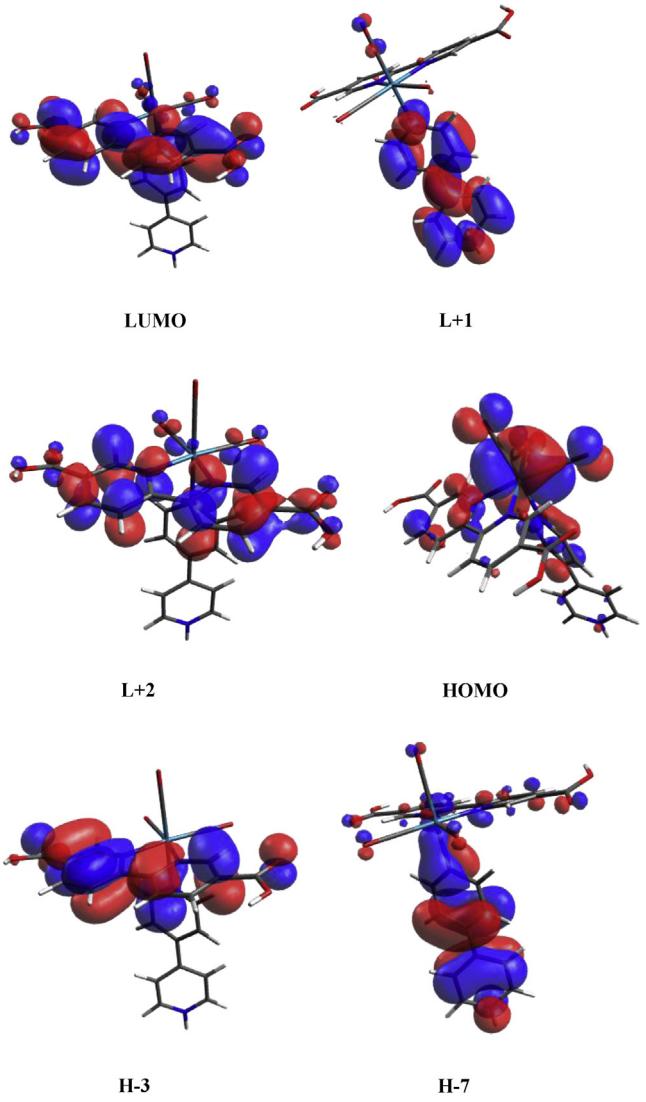

Fig. 5. Molecular orbital diagrams for complex **(ReL)H$_3^{2+}$**. HOMO and L+1 are the major MOs involved in the lower energy transition (λ_{max} = 371 nm), while orbitals LUMO, L+2, H-3 and H-7 are the major contributors to the electronic spectrum in the 220–350 nm range.

The calculated electronic spectra of **(ReL)**$^-$, **(ReL)H**, **(ReL)H$_2^+$** and **(ReL)H$_3^{2+}$** are simulated from the theoretical results to ease the comparison with experimental data. The simulation was performed with the following function [75]:

$$I(E) = \frac{1}{\pi}\sum_i \frac{\sigma \cdot f_i}{\sigma^2 + (E-\varepsilon_i)^2}$$

where I is the peak intensity in the spectrum at a given energy E, ε_i is the calculated energy of the electronic transition, σ is the band width and f_i is the intensity of the electronic transition. In the absence of a theoretical basis, σ is often used as a fitted parameter. The simulations are shown in Fig. 6 in comparison with the spectra of the contributing species to the spectral changes of protonation studies (Fig. 2). The comparison is quite satisfactory and the simulated spectra of **(ReL)**$^-$, **(ReL)H**, **(ReL)H$_2^+$** and **(ReL)H$_3^{2+}$** follow approximately the trend of the spectral changes in Fig. 1 in the UV–vis region. Moreover, the displacement of the lower energy band, from ~362 nm at neutral pH to 376 nm at pH = 1 (Fig. 1b) is in

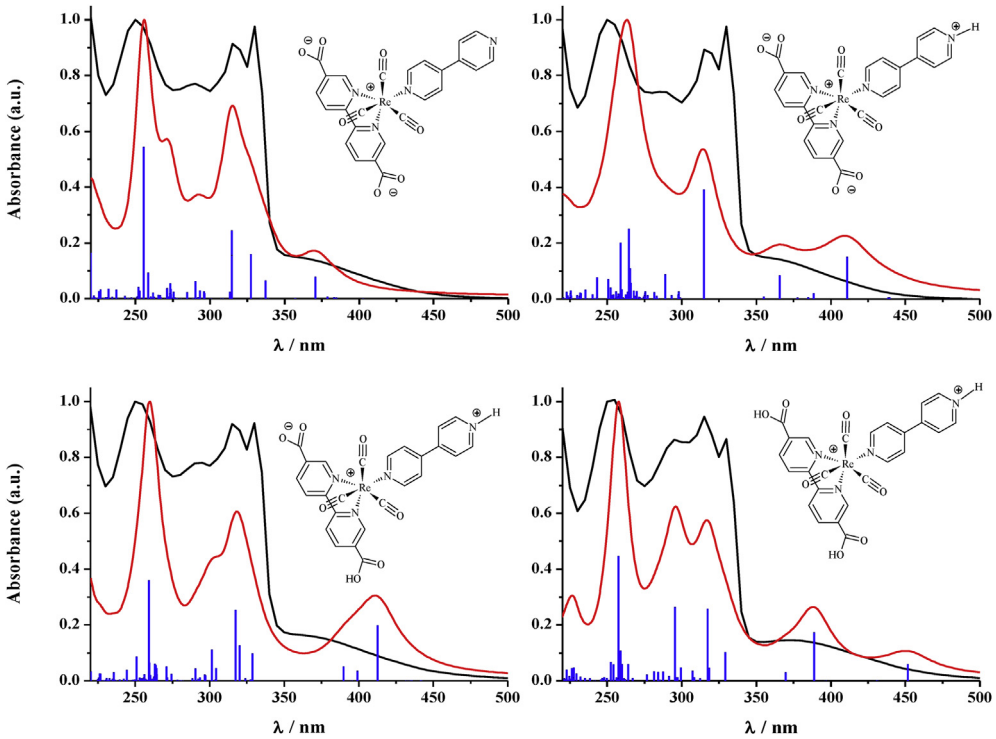

Fig. 6. Comparison of the spectral shapes for the four species obtained from chemometric analysis of UV–vis spectral changes of Fig. 1a and b (black lines) with TD-DFT calculated electronic transitions (blue lines) and simulated spectra (red lines) for **(ReL)**$^-$, **(ReL)H**, **(ReL)H$_2^+$** and **(ReL)H$_3^{2+}$**.

agreement with the change in the nature of the lower energy band (predicted by TD-DFT calculations) from $MLLCT_{Re(CO)3\rightarrow dcbpy}$ in **(ReL)**$^-$ (λ_{max} = 371 nm) to $MLLCT_{Re(CO)3\rightarrow bpy}$ in **(ReL)H$_3^{2+}$** (λ_{max} = 389 nm). It is to noteworthy that the band width, σ, was chosen to approximately fit the experimental absorption peaks in the 250–350 nm region by the calculated energies. By choosing a fixed value of σ, a reasonable good agreement between theory and experiment is observed in that wavelength region though a lesser agreement is found at the region of the low energy band ($\lambda > 350$ nm). By choosing a higher value of σ, a better agreement can be achieved in the region of the low energy band, however losing the relative good agreement between calculated and observed spectra in the 250–350 nm region. This is a consequence of the band width being dependent on a particular electronic transition rather than being the same for the whole spectrum.

4. Conclusion

A new Re(I) complex, $Bu_4N[(bpy)Re(CO)_3(dcbpy)]$, has been obtained successfully and characterized by ^{1}H NMR, FTIR and ESI. Due to its zwitterionic structure, it has a good solubility in water. From protonation studies, three p*K*a values could be obtained from chemometric analysis of pH-dependent spectral changes. Those values of p*K*a were assigned to the protonation of 4,4′-bipyridine ligand (pKa_1 = 5.0) and to the acid–base equilibrium of the two carboxylate groups (pKa_2 = 3.0 and pKa_3 = 2.0) in dcbpy. TD-DFT calculations showed that at neutral pH, where **(ReL)**$^-$ is the predominant species, the lower energy band of the complex has $MLLCT_{Re(CO)3\rightarrow dcbpy}$ character while at pH = 1, where **(ReL)H$_3^{2+}$** is the most abundant, the nature of the lower energy band switches to $MLLCT_{Re(CO)3\rightarrow bpy}$. This change in the nature of the lower energy band is responsible for the overall spectral changes in the 350–500 nm range after protonation of the Re(I) complex. The calculated electronic spectra of **(ReL)**$^-$, **(ReL)H**, **(ReL)H$_2^+$** and **(ReL)H$_3^{2+}$** were in good agreement with the spectral profiles of the contributing species to the spectral changes of protonation studies.

Acknowledgments

This work was supported in part by ANPCyT (PICT 1435), CONICET (PIP 0389), and Universidad Nacional de La Plata (UNLP X533) of Argentina. H.H.M.S. thank CONICET for research scholarship. FTIR measurements were performed at Dr. Adela Croce's laboratory. We thank Dr. A.C. for hosting our visits to her laboratory. MCR-ALS methods were implemented through *Kinesim* 9.5. We thank Dr. Fernando García Einschlag for the use of that software. C.A.F. acknowledges Universidad Nacional de Catamarca for computing time. G.P, R.E.-B., G.T.R. and E.W. are Research Members of CONICET (Argentina).

Appendix A. Supplementary data

Supplementary data related to this article can be found at http://dx.doi.org/10.1016/j.jorganchem.2013.08.038.

References

[1] G. Ruiz, E. Wolcan, M.R. Féliz, J. Photochem. Photobiol. A 101 (1996) 119.
[2] D.J. Stufkens, A. Vlček Jr., Coord. Chem. Rev. 177 (1998) 127.
[3] M.A. Fox, M. Chanon, Photoinduced Electron Transfer, Elsevier, Amsterdam, 1988.
[4] V. Balzani, F. Bolletta, M. Gandolfi, M. Maestri, in: Organic Chemistry and Theory, Springer, Berlin/Heidelberg, 1978, p. 1.
[5] M. Grätzel, Energy Resources Through Photochemistry and Catalysis, Academic Press, New York, 1983.
[6] K. Kalyanasundaram, Coord. Chem. Rev. 46 (1982) 159.
[7] K. Kalyanasundaram, M. Grätzel, Photosensitization and Photocatalysis Using Inorganic and Organometallic Compounds, Kluwer Academic Publishers, Dordrecht, 1993.
[8] L. Sacksteder, M. Lee, J.N. Demas, B.A. DeGraff, J. Am. Chem. Soc. 115 (1993) 8230.

[9] V.W.-W. Yam, K.M.-C. Wong, V.W.-M. Lee, K.K.-W. Lo, K.-K. Cheung, Organometallics 14 (1995) 4034.
[10] D.I. Yoon, C.A. Berg-Brennan, H. Lu, J.T. Hupp, Inorg. Chem. 31 (1992) 3192.
[11] J.C. Calabrese, W. Tam, Chem. Phys. Lett. 133 (1987) 244.
[12] T.T. Ehler, N. Malmberg, K. Carron, B.P. Sullivan, L.J. Noe, J. Phys. Chem. B 101 (1997) 3174.
[13] V.W.-W. Yam, V.C.-Y. Lau, K.-K. Cheung, J. Chem. Soc. Chem. Commun. (1995) 259.
[14] B. Higgins, B.A. DeGraff, J.N. Demas, Inorg. Chem. 44 (2005) 6662.
[15] U.N. Fagioli, F.S. García Einschlag, C.J. Cobos, G.T. Ruiz, M.R. Féliz, E. Wolcan, J. Phys. Chem. A 115 (2011) 10979.
[16] S.C. Bottorff, A.L. Moore, A.R. Wemple, D.-K. Bučar, L.R. MacGillivray, P.D. Benny, Inorg. Chem. 52 (2013) 2939.
[17] A. Vlček, in: A.J. Lees (Ed.), Photophysics of Organometallics, Springer, Berlin/Heidelberg, 2010, p. 73.
[18] A. Kumar, S.-S. Sun, A. Lees, in: A.J. Lees (Ed.), Photophysics of Organometallics, Springer, Berlin/Heidelberg, 2010, p. 37.
[19] M.-W. Louie, T.T.-H. Fong, K.K.-W. Lo, Inorg. Chem. 50 (2011) 9465.
[20] K. Lo, in: A.J. Lees (Ed.), Photophysics of Organometallics, Springer, Berlin/Heidelberg, 2010, p. 73.
[21] K.K.-W. Lo, A.W.-T. Choi, W.H.-T. Law, Dalton Trans. 41 (2012) 6021.
[22] G.T. Ruiz, M.P. Juliarena, R.O. Lezna, E. Wolcan, M.R. Feliz, G. Ferraudi, Dalton Trans. (2007) 2020.
[23] S.P. Foxon, M.A.H. Alamiry, M.G. Walker, A.J.H.M. Meijer, I.V. Sazanovich, J.A. Weinstein, J.A. Thomas, J. Phys. Chem. A 113 (2009) 12754.
[24] J. Bhuvaneswari, A.K. Fathima, S. Rajagopal, J. Photochem. Photobiol. A 227 (2012) 38.
[25] M. Cattaneo, F. Fagalde, C.D. Borsarelli, N.s.E. Katz, Inorg. Chem. 48 (2009) 3012.
[26] M. Cattaneo, F. Fagalde, N.E. Katz, Inorg. Chem. 45 (2006) 6884.
[27] M. Cattaneo, F. Fagalde, N.E. Katz, C.D. Borsarelli, T. Parella, Eur. J. Inorg. Chem. 2007 (2007) 5309.
[28] R.-J. Lin, K.-S. Lin, I.J. Chang, Inorg. Chim. Acta 242 (1996) 179.
[29] F. Ragone, G.T. Ruiz, O.E. Piro, G.A. Echeverría, F.M. Cabrerizo, G. Petroselli, R. Erra-Balsells, K. Hiraoka, F.S. García Einschlag, E. Wolcan, Eur. J. Inorg. Chem. (2012) 4801.
[30] A. Juris, S. Campagna, I. Bidd, J.M. Lehn, R. Ziessel, Inorg. Chem. 27 (1988) 4007.
[31] C. Hop, D. Saulys, D. Gaines, J. Am. Soc. Mass Spectrom. 6 (1995) 860.
[32] G. Petroselli, M.K. Mandal, L.C. Chen, G.T. Ruiz, E. Wolcan, K. Hiraoka, H. Nonami, R. Erra-Balsells, J. Mass Spectrom. 47 (2012) 313.
[33] G.J. Van Berkel, S.A. McLuckey, G.L. Glish, Anal. Chem. 64 (1992) 1586.
[34] F. García Einschlag, Kinesim 9.5: Obra de software. Dirección Nacional del Derecho de Autor, Argentina, 2005. Expediente No. 395814.
[35] C. Ruckebusch, S. Aloise, L. Blanchet, J.P. Huvenne, G. Buntinx, Chemom. Intell. Lab. Syst. 91 (2008) 17.
[36] R. Tauler, Chemom. Intell. Lab. Syst. 30 (1995) 133.
[37] M. Goez, I. Sartorius, J. Am. Chem. Soc. 115 (1993) 11123.
[38] M. Blanco, A.C. Peinado, J. Mas, Anal. Chim. Acta 544 (2005) 199.
[39] M. Meloun, J. Čapek, P. Mikšik, R.G. Brereton, Anal. Chim. Acta 423 (2000) 51.
[40] A. de Juan, R. Tauler, Anal. Chim. Acta 500 (2003) 195.
[41] P. Gemperline, E. Cash, Anal. Chem. 75 (2003) 4236.
[42] P. Hohenberg, W. Kohn, Phys. Rev. 136 (1964) B864.
[43] W. Kohn, L.J. Sham, Phys. Rev. 140 (1965) A1133.
[44] R.G. Parr, W. Yang, Density Functional Theory of Atoms and Molecules, Oxford University Press, 1989.
[45] M.J. Frisch, G.W. Trucks, H.B. Schlegel, G.E. Scuseria, M.A. Robb, J.R. Cheeseman, G. Scalmani, V. Barone, B. Mennucci, G.A. Petersson, H. Nakatsuji, M. Caricato, X. Li, H.P. Hratchian, A.F. Izmaylov, J. Bloino, G. Zheng, J.L. Sonnenberg, M. Hada, M. Ehara, K. Toyota, R. Fukuda, J. Hasegawa, M. Ishida, T. Nakajima, Y. Honda, O. Kitao, H. Nakai, T. Vreven, J.J.A. Montgomery, J.E. Peralta, F. Ogliaro, M. Bearpark, J.J. Heyd, E. Brothers, K.N. Kudin, V.N. Staroverov, T. Keith, R. Kobayashi, J. Normand, K. Raghavachari, A. Rendell, J.C. Burant, S.S. Iyengar, J. Tomasi, M. Cossi, N. Rega, J.M. Millam, M. Klene, J.E. Knox, J.B. Cross, V. Bakken, C. Adamo, J. Jaramillo, R. Gomperts, R.E. Stratmann, O. Yazyev, A.J. Austin, R. Cammi, C. Pomelli, J.W. Ochterski, R.L. Martin, K. Morokuma, V.G. Zakrzewski, G.A. Voth, P. Salvador, J.J. Dannenberg, S. Dapprich, A.D. Daniels, O. Farkas, J.B. Foresman, J.V. Ortiz, J. Cioslowski, D.J. Fox, Gaussian, Inc., Wallingford, CT, 2010.
[46] A.D. Becke, J. Chem. Phys. 98 (1993) 5648.
[47] C. Lee, W. Yang, R.G. Parr, Phys. Rev. B 37 (1988) 785.
[48] T.H. Dunning Jr., P.J. Hay, in: H.F. Schaefer III (Ed.), Methods of Electronic Structure Theory, Plenum Press, 1977.
[49] P.J. Hay, W.R. Wadt, J. Chem. Phys. 82 (1985) 270.
[50] P.J. Hay, W.R. Wadt, J. Chem. Phys. 82 (1985) 299.
[51] W.R. Wadt, P.J. Hay, J. Chem. Phys. 82 (1985) 284.
[52] R. Bauernschmitt, R. Ahlrichs, Chem. Phys. Lett. 256 (1996) 454.
[53] M.E. Casida, C. Jamorski, K.C. Casida, D.R. Salahub, J. Chem. Phys. 108 (1998) 4439.
[54] R.E. Stratmann, G.E. Scuseria, M.J. Frisch, J. Chem. Phys. 109 (1998) 8218.
[55] V. Barone, M. Cossi, J. Phys. Chem. A 102 (1998) 1995.
[56] M. Cossi, V. Barone, J. Chem. Phys. 115 (2001) 4708.
[57] B. Mennucci, J. Tomasi, J. Chem. Phys. 106 (1997) 5151.
[58] M.V. Werrett, D. Chartrand, J.D. Gale, G.S. Hanan, J.G. MacLellan, M. Massi, S. Muzzioli, P. Raiteri, B.W. Skelton, M. Silberstein, S. Stagni, Inorg. Chem. 50 (2011) 1229.
[59] W. Yawei, S. Wenjian, Y. Yun, C. Xiaoyun, in: ICBBE 2009. 3rd International Conference on, 2009, 2009, p. 1.
[60] J. Guerrero, O.E. Piro, E. Wolcan, M.R. Feliz, G. Ferraudi, S.A. Moya, Organometallics 20 (2001) 2842.
[61] A. Garrido Frenich, D. Picón Zamora, J.L. Martínez Vidal, M. Martínez Galera, Anal. Chim. Acta 449 (2001) 143.
[62] M.K. Nazeeruddin, K. Kalyanasundaram, Inorg. Chem. 28 (1989) 4251.
[63] M.K. Nazeeruddin, S.M. Zakeeruddin, R. Humphry-Baker, M. Jirousek, P. Liska, N. Vlachopoulos, V. Shklover, C.-H. Fischer, M. Grätzel, Inorg. Chem. 38 (1999) 6298.
[64] S. Zhang, R. Shepherd, Trans. Met. Chem. (Lond.) 17 (1992) 199.
[65] Y. Gao, S. Sun, K. Han, Spectrochim. Acta A 71 (2009) 2016.
[66] A. Vlcek Jr., S. Zális, Coord. Chem. Rev. 251 (2007) 258.
[67] J. Dietrich, U. Thorenz, C. Förster, K. Heinze, Inorg. Chem. 52 (2013) 1248.
[68] D. Chartrand, C.A. Castro Ruiz, G.S. Hanan, Inorg. Chem. 51 (2012) 12738.
[69] C. Zhao, C.S. Kambara, Y. Yang, A.L. Kaledin, D.G. Musaev, T. Lian, C.L. Hill, Inorg. Chem. 52 (2013) 671.
[70] C.B. Anderson, A.B.S. Elliott, C.J. McAdam, K.C. Gordon, J.D. Crowley, Organometallics 32 (2013) 788.
[71] L. Yang, A.-M. Ren, J.-K. Feng, X.-D. Liu, Y.-G. Ma, H.-X. Zhang, Inorg. Chem. 43 (2004) 5961.
[72] L. Yang, A.-M. Ren, J.-K. Feng, X.-J. Liu, Y.-G. Ma, M. Zhang, X.-D. Liu, J.-C. Shen, H.-X. Zhang, J. Phys. Chem. A 108 (2004) 6797.
[73] S. Záliš, C.J. Milne, A. El Nahhas, A.M. Blanco-Rodríguez, R.M. van der Veen, A. Vlček, Inorg. Chem. 52 (2013) 5775.
[74] E. Wolcan, G. Torchia, J. Tocho, O.E. Piro, P. Juliarena, G. Ruiz, M.R. Féliz, J. Chem. Society Dalton Trans. (2002) 2194.
[75] R. Pis-Diez, B.S. Parajón-Costa, C.A. Franca, O.E. Piro, E.E. Castellano, A.C. González-Baró, J. Mol. Struct. 975 (2010) 303.